Indian J. Phys. **73A** (1), 55–71 (1999)

IJP A
- an international journal

HERA physics—an overview of experimental and theoretical results

Rahul Basu
The Institute of Mathematical Sciences,
Chennai (Madras)-600 113, India

Abstract : In this talk I review the low x QCD experimental results from HERA and their theoretical underpinnings. In particular, I discuss the structure function F_2, large rapidity gap events, pomeron structure functions and J/ψ production.

Keywords : HERA, structure functions, deep inelastic scattering

PACS Nos. : 12.38.–t, 13.60.Hb

1. Introduction

The electron (positron)-proton collider facility at DESY, nicknamed HERA (for Hadron Electron Ring Accelerator) has, since its inception in 1992, given many new and interesting results from the two experiments H1 and ZEUS. These experiments have thrown up a wealth of new theoretical issues pertaining to low x QCD. These experiments cover both the deep-inelastic region (DIS) and the photoproduction region. The basic interaction picture is the usual DIS diagram shown in Figure 1 for the process

$$e(k)+p(p) \rightarrow e(k')+X.$$

The following kinematic variables completely describe the process :

$$s = (k+p)^2 \simeq 4E_eE_p, \tag{1}$$

$$Q^2 = -q^2 \simeq 2E_eE_{e'}(1+\cos\theta), \tag{2}$$

$$y = \frac{p.q}{p.k} \simeq 1-\frac{E_{e'}}{2E_e}(1-\cos\theta), \tag{3}$$

$$x = \frac{Q^2}{2p.q} \simeq \frac{Q^2}{ys}, \tag{4}$$

$$W = (q+p)^2 \simeq -Q^2+ys. \tag{5}$$

Here s is the CM Energy squared, $E_e(E_e')$ is the energy of the initial (scattered) electron, θ the angle of the scattered electron in the lab frame with respect to the proton direction, Q^2

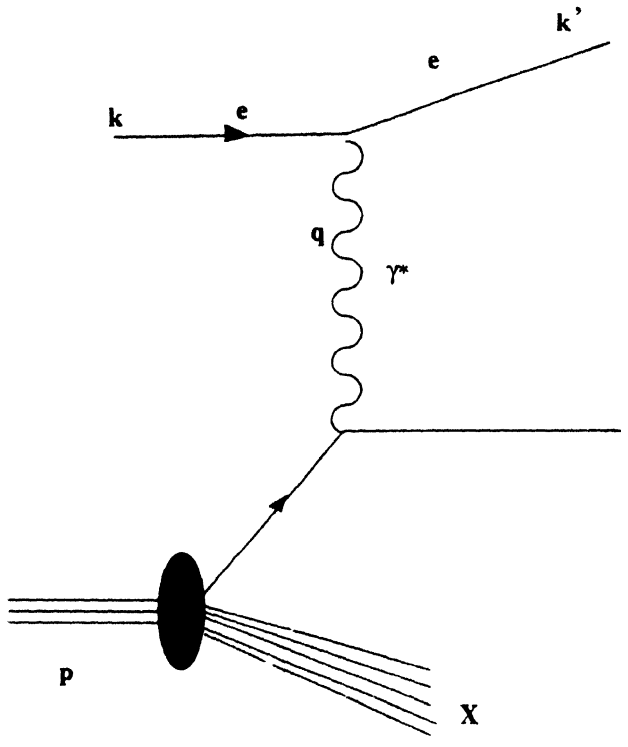

Figure 1. The basic DIS diagram with kinematic variables labelled.

is the negative of the momentum transfer squared to the proton, y is the fraction of the electron energy carried by the virtual photon in the proton rest frame, the Bjorken variable x is the fraction of the proton energy carried by the struck quark and W is the hadronic invariant mass. The masses of all particles are neglected.

At HERA, a 27 GeV electron beam collides head-on with an 820 GeV proton beam giving

$$s \simeq 4E_eE_p \sim 10^5 \text{GeV}^2,$$

which is much larger than hitherto obtained at fixed target experiments. As a result the two experiments H1 and ZEUS can measure the structure function F_2 in a completely new (x, Q^2) domain (see Figure 2).

The Born cross section for single photon exchange in DIS is given by

$$\frac{d^2\sigma}{dxdQ^2} = \frac{2\pi\alpha^2}{Q^2x}\left[2(1-y)+\frac{y^2}{1+R}\right]F_2(x,Q^2), \tag{6}$$

where R is the photoproduction cross section ratio for longitudinal and transverse polarised photon, $R = \sigma_L/\sigma_T$. R has not been measured at HERA; therefore a QCD prescription based on parametrisation of parton densities is used. Q^2 is directly measured from the scattered

electron but x is calculated from Q^2 and y and therefore depends on the experimental resolution of y.

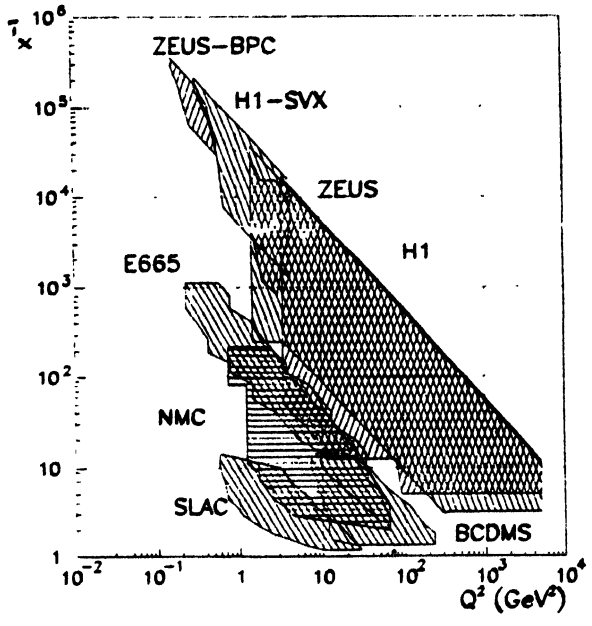

Figure 2. Phase space coverage of the F_2 measurements (from [13]).

2. Measurement of $F_2^p(x, Q^2)$

The data for F_2^p from H1 and ZEUS [1,2] is shown in Figures 3, 4 and 5, along with some of the older fixed target data. It is clear that at fixed Q^2, F_2 rises with decreasing x down to

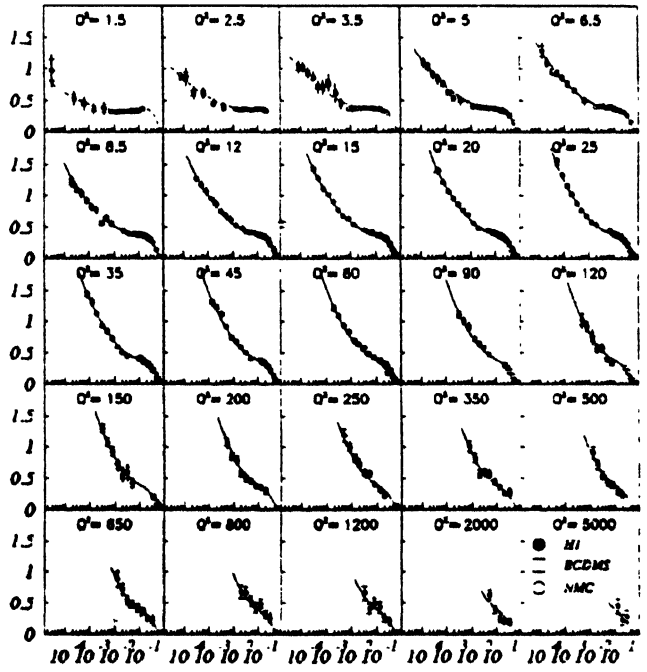

Figure 3. $F_2(x, Q^2)$ as a function of x. The curves are the NLO QCD fit for $Q^2 \geq 5$ GeV^2. Curves below 5 GeV^2 are obtained by backward evolution. (from [1]).

the smallest Q^2, the steepness of the rise decreasing with decreasing Q^2. Similarly at fixed $x < 0.1$ F_2 rises with Q^2, the rise becoming steeper as x decreases. (We shall henceforth drop the superscript p on F_2 since all our discussion henceforth will refer to the structure function of the proton). In fact, as seen in Figure 4, upto Q^2 ~0.85 GeV^2 the data favour a parametrisation based on a soft pomeron such as that suggested by Donnachie and Landshoff [3]. For larger values of Q^2 ($Q^2 > 1.0$ GeV^2) the usual QCD based parametrisations of GRV or MRS [4,5] give a good description of the data.

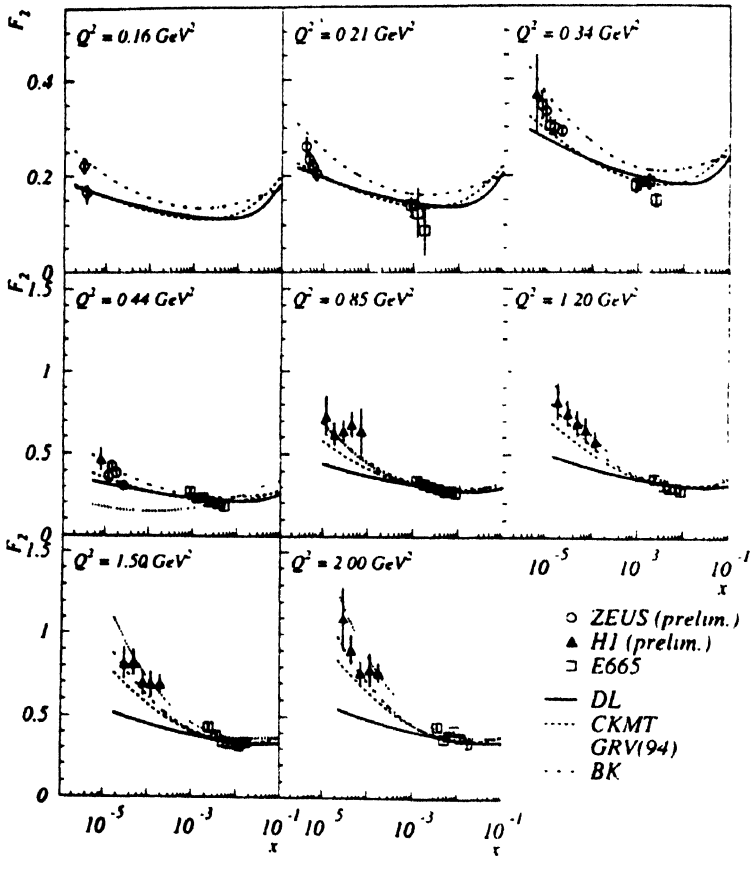

Figure 4. $F_2(x, Q^2)$ as a function of x for low Q^2 compared with model predictions. (from [13]).

The behaviour of F_2 as a function of Q^2 for selected values of x is presented in Figure 5. The growth of the structure function with Q^2 for $x < 0.01$ over three orders of magnitude in Q^2 is clearly seen. With the new data from HERA the gap between fixed target and the HERA experiments has been filled and the remarkable agreement with a NLO QCD fit performed by H1 over three decades in Q^2 and over four decades in x is clearly seen.

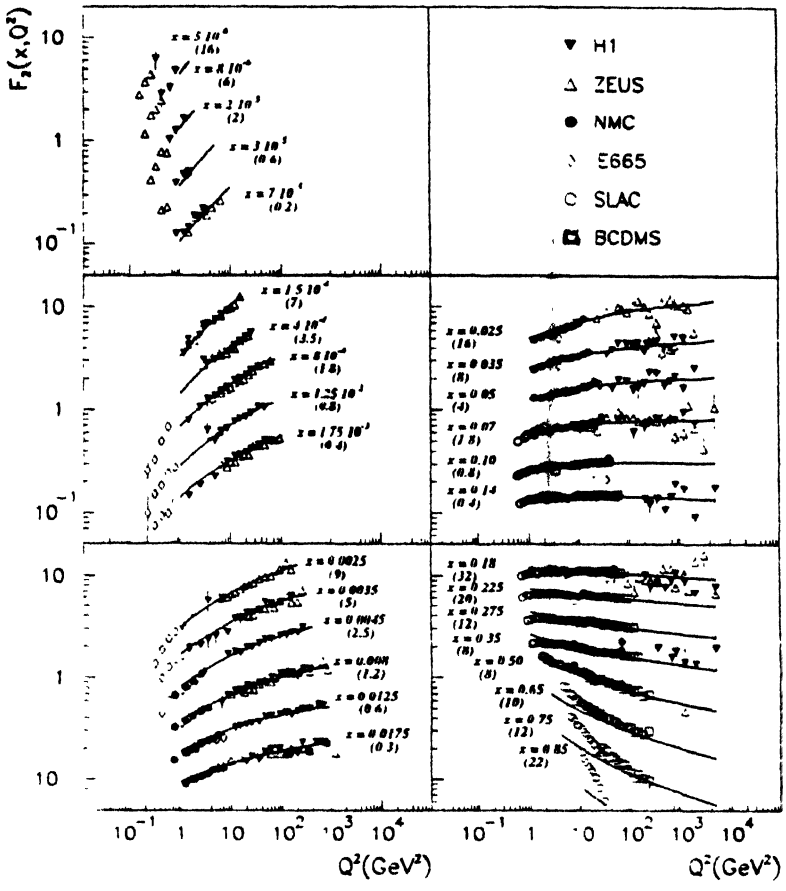

Figure 5. Compilation of F_2 measurements as a function Q^2 for selected values of x. The numbers in parenthesis are the scaling factors by which the value of F_2 has been multiplied in the plot. The curves are a NLO QCD fit by H1. (from [13]).

The H1 experiment has parametrised the rise of F_2 with x by $F \sim x^{-\lambda}$ at fixed Q^2 values. The result for λ as a function of Q^2 is shown in Figure 6. It is clear from the figure that λ increases with increasing Q^2 reaching a value of around 0.4–0.5 around $Q^2 \sim 10^2$–10^3 GeV^2.

3. The rise of F_2 and perturbative QCD

The structure function $F_2(x, Q^2)$ is given in terms of the parton distributions

$$\frac{F_2(x, Q^2)}{x} \equiv \sum_{i=1}^{n_f} e_i^2 C_i \otimes (q_i + \bar{q}_i) + C_g \otimes g. \tag{7}$$

The evolution of the structure function F_2 as a function of Q^2 is governed, in perturbative QCD, by the Dokshitser-Gribov-Lipatov-Altarelli-Parisi (DGLAP) eqs. [6,7],

$$\frac{\partial}{\partial \ln Q^2}\begin{pmatrix} q \\ g \end{pmatrix} = \frac{\alpha_s(Q^2)}{2\pi}\begin{bmatrix} P_{qq} & P_{qg} \\ P_{gq} & P_{gg} \end{bmatrix} \otimes \begin{pmatrix} q \\ \end{pmatrix} \tag{8}$$

Here q and g are the quark and gluon distributions, $\otimes$ denotes convolution with respect to x, *i.e.* $[f \otimes g]\,(x) \equiv \int_x^1 \frac{dy}{y} f\left(\frac{x}{y}\right) g(y)$, n_f is the number of flavours of quarks, e_i is the electric charge of the quark q_i. The coefficient functions C's at leading order are

$$C_i(x,Q^2) = \delta(1-x);\ C_g(x,Q^2) = 0. \tag{9}$$

At higher orders, they depend on the specific factorization scheme. In the common parton scheme the above remains true to all orders.

The splitting functions have the expansion

$$P_{ij}(x, Q^2) = \frac{\alpha_s}{2\pi} P_{ij}^{(1)}(x) + \left(\frac{\alpha_s}{2\pi}\right)^2 P_{ij}^{(2)}(x) + \cdots \tag{10}$$

The first two terms above define the NLO DGLAP evolution.

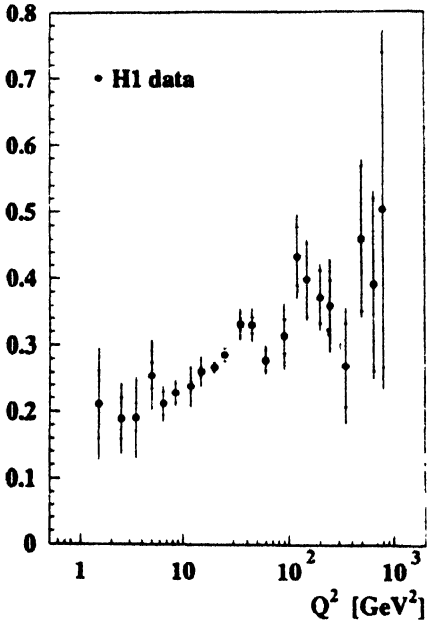

Figure 6. Variation of the exponent λ from fits of the form $F_2 \sim x^{-\lambda}$ at fixed Q^2 values and $x < 0.1$. (from [1]).

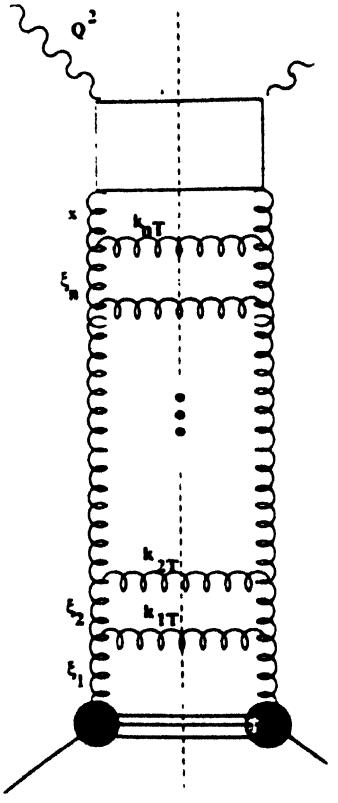

Figure 7. A gluon ladder diagram that contributes to the DLL or BFKL ladder summations.

The rise of F_2 as a function of x is explained by the usual DGLAP evolution and also by more non-conventional dynamics like the BFKL evolution [8]. Let us briefly review the two different approaches.

To understand the leading log summation technique in the DGLAP approach, we use the Dokshitzer method [6]. He showed that the GLAP summation of the $(\alpha_s \log Q^2)^n$ terms amounts to a sum of gluon ladder diagrams of the type shown in Figure 7 with n gluon rungs. The form of the gluon splitting function $P_{gg} \sim 6/x$ for small x gives the evolution of the gluon distribution function as

$$xg(x, Q^2) = \sum_n \left(\frac{3\alpha_s}{\pi}\right)^n \int^{Q^2} \frac{dk_{nT}^2}{k_{nT}^2} \cdots \int^{k_{3T}^2} \frac{dk_{2T}^2}{k_{2T}^2} \int^{k_{2T}^2} \frac{dk_{1T}^2}{k_{1T}^2}$$

$$\times \int_x^1 \frac{d\xi_n}{\xi_n} \cdots \int_{\xi_{3n}}^1 \frac{\xi_2}{\xi_2} \int_{\xi_2}^1 \frac{\xi_1}{\xi_1} \xi_1 g(\xi_1, Q_0^2). \tag{11}$$

It is clear that the $(\log Q^2)^n$ builds up from the nested k integrations. In fact this contribution comes from a region where the transverse momentum of the emitted gluons are strongly ordered

$$Q^2 >> k_{nT}^2 >> \cdots >> k_{2T}^2 >> k_{1T}^2 \tag{12}$$

Similarly, the $(\log (1/x))^n$ term comes from the region where the longitudinal momentum fractions are strongly ordered

$$x << \xi_n << \cdots << \xi_2 << \xi_1. \tag{13}$$

In the region of small x, the $\log (1/x)$ terms have also to be summed. With the assumption of $\xi_1 g(\xi_1, Q_0^2)$ approaching a constant, say G_0 the result we get is

$$xg(x, Q^2) \sim \sum_n \left(\frac{3\alpha_s}{\pi}\right)^n \left\{\frac{1}{n!}\left[\log\left(\frac{Q^2}{Q_0^2}\right)\right]^n\right\} \left\{\frac{1}{n!}\left[\log\left(\frac{1}{x}\right)\right]^n G_0\right\} \tag{14}$$

$$\sim G_0 \exp\left\{2\left[\frac{3\alpha_s}{\pi} \log\left(\frac{Q^2}{Q_0^2}\right) \log\left(\frac{1}{x}\right)\right]^{\frac{1}{2}}\right\}$$

in the limit of large Q^2 and small x.

This is an example of an all order double leading log (DLL) summation of $\alpha_s \log Q^2 \log(1/x)$ obtained by summing the strongly ordered gluon ladder diagrams as we have just explained. It tells us that as x decreases, $xg(x, Q^2)$ increases faster than any power of $\log(1/x)$ but slower than any power of $1/x$.

If $k_{iT} \approx k_{i+1T}$ then we lose one power of $\log Q^2$. However, at small x, this can be compensated by a large $\log (1/x)$ factor. Relaxing the strong ordering constraint on the k_T's and summing just the $\log (1/x)$ in the small x region will give us the leading log summation in $\log(1/x)$ instead of DLL and we get

$$xg(x, Q^2) \approx \sum_n \left(\frac{3\alpha_s}{\pi}\right)^n \frac{1}{n!}\left[c \log\left(\frac{1}{x}\right)\right]^n$$
$$\sim \exp\left[\lambda \log\left(\frac{1}{x}\right)\right]$$
$$\sim x^{-\lambda}, \tag{15}$$

where $\lambda = (3\alpha_s/\pi)c$. This difficult summation was done rigorously by Balitskij, Fadin, Kuraev and Lipatov (BFKL) [8]. The constant $c = 4 \log 2$ and so, for $\alpha_s \approx 0.2$, $\lambda \approx 0.5$. We have highly simplified the discussion of the BFKL equation, and in practise one needs to work in terms of the unintegrated gluon distribution $f(x, k_T^2)$ and integrate $f(x, k_T^2)/k_T^2$ to get the final gluon distribution.

We thus have two different predictions for the rise of F_2, the DLL (from the DGLAP evolution equations) and the BFKL. In principle it should therefore be possible to distinguish between these predictions by looking at the F_2 data from HERA. Unfortunately this is not that simple. The steepness of the rise of F_2 with decreasing x can be controlled by varying Q_0^2, or the starting distribution $g(\xi_1, Q_0^2)$. In addition, the set of equations based only on F_2 measurements is underconstrained and one needs one other measurement like the longitudinal structure function F_L in order to constrain the system fully.

The net consequence of the above is that the present data on F_2 does not distinguish between the BFKL and DGLAP (or for that matter the CCFM which embodies both) predictions.

We would like to mention here a suggestion by Mueller [9] on measuring an observable that is less inclusive than the F_2 measurement (in which none of the properties of the hadronic final state is measured). He suggests studying DIS events at small x containing an identified high-energy jet emitted close to the jet of proton fragments (see Figure 8). The identified jet originates from the parton labelled a. If we study events with x_j large (≥ 0.05) and x very small ($\approx 10^{-4}$) the ratio x/x_j will be sufficiently small to reveal the $(x/x_j)^{-\lambda}$ behaviour of the BKFL ladder. Details may be found in the references mentioned above. This study is currently under way and preliminary results are reported in [10].

The behaviour of F_2 as a function of both Q^2 and x (for large Q^2 and small x) can be neatly combined through the double asymptotic scaling analysis of Ball and Forte [11].

They use the two variables

$$\sigma \equiv \sqrt{\log(x_0/x)\log(\alpha_s(Q_0)/\alpha_s(Q))}, \quad \rho \equiv \sqrt{\frac{\log(x_0/x)}{\log(\alpha_s(Q_0)/\alpha_s(Q))}} \tag{16}$$

with $\alpha_s(Q)$ the strong coupling constant evaluated upto two loops.

The parameters x_0 and Q_0^2 have to be determined experimentally. Q_0^2 is found to be 2.5 GeV^2 and $\lambda_0 = 0.1$. (See, for example [1]). F_2 is rescaled by the leading asymptotic factors

$$R_F(\sigma, \rho) = 8.1 \exp\left(-2\gamma\sigma + \omega\frac{\sigma}{\rho} + \frac{1}{2}\log(\gamma\sigma) + \log\left(\frac{\rho}{\gamma}\right)\right)/\xi_F \quad (17)$$

and
$$R'_F(\sigma, \rho) = R_F \exp(2\gamma\sigma), \quad (18)$$

where
$$\xi_F = 1 + \left((\xi_1 + \xi_2)\alpha_s(Q) - \xi_1\alpha_s(Q_0)\right)(\rho/(2\pi\gamma)). \quad (19)$$

The above constants are $\xi_1 = (206n_f/27 + 6b_1/b_0)/b_0$, $\xi_2 = 13$, $b_0 = 11 - 2n_f/3$, $w = (11 + 2n_f/27)/b_0$ and $b_1 = 102 - 38n_f/3$. Also n_f is the number of flavours and $\gamma = \sqrt{12/b_0}$.

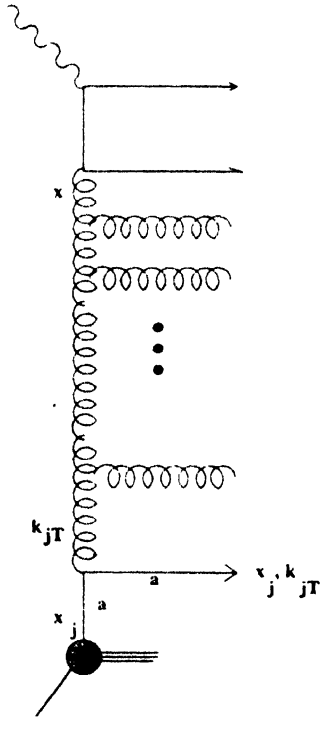

Figure 8. A ladder diagram contributing to an identified forward jet as discussed in the text.

Thus the function $\log(R'_F F_2)$ is predicted to rise linearly with s and $R_F F_2$ is expected to be independent of ρ and σ.

Figure 9 shows the data for these two predictions. The first graph is for $Q^2 \geq 3.5$ GeV^2. Approximate scaling is observed for $Q \geq 5$ GeV^2 and $\rho \geq 2$. At high ρ and low Q^2, the data tends to violate the predicted scaling behaviour. The second graph shows the appropriate data for $\rho \geq 2$ and $Q^2 \geq 5$ GeV^2 as a function of σ The predicted linear rise is seen with slope of $2.50 \pm 0.02 \pm 0.06$ in good agreement with the QCD expectation of 2.4 for 4 flavours.

Thus in the low x, high Q^2 region beyond $Q^2 \geq 5$ GeV^2, scaling is seen in the two variables ρ and σ. The prediction of double scaling is in very good agreement in this region

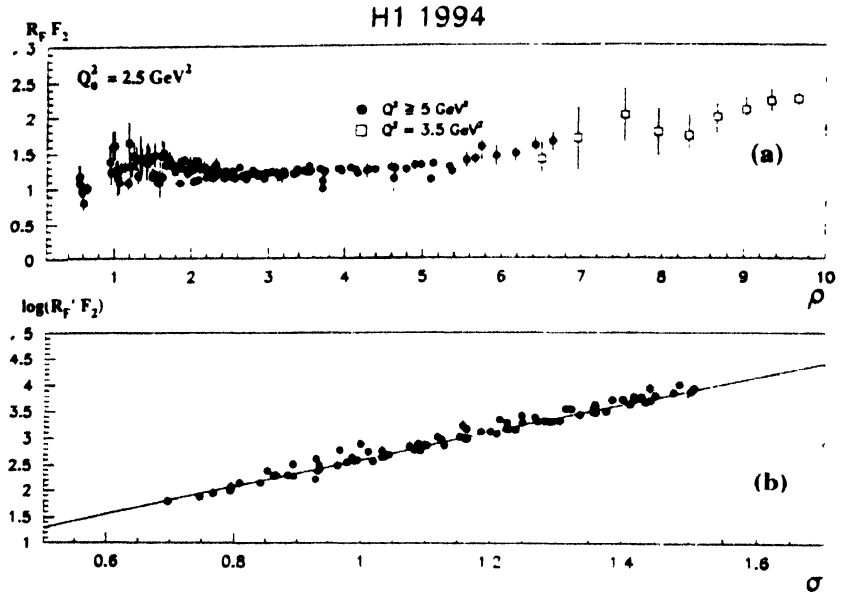

Figure 9. The rescaled structure functions (a) $R_F F_2$ *vs.* ρ and (b) log $(R'_F F_2)$ *vs* σ as explained in the text. Only data with $Q^2 \geq 5$ GeV^2 and $\rho > 2$ are shown in (b) (from [11])

with experiment. Beyond the double scaling region, the evolution continues to be in excellent agreement with the full NLO QCD evolution prediction.

To summarise this section, the structure function F_2 has been found to rise steeply with decreasing x down to Q^2 as low as 0.85 GeV^2. This rise can be parametrised by a form $x^{-\lambda}$ where λ is found to be a function of Q^2 and reaches a value of around 0.4–0.5 around 1000 GeV^2. This behaviour is described very well by conventional NLO QCD (through the DGLAP equation). However this does not rule out the existence of non-conventional dynamics like BFKL because the system is underconstrained. Thus some other measurement which is less inclusive than F_2 like the forward jet mentioned above, or a measurement of the longitudinal structure function F_L is required. In any case, some new physics must take over at sufficiently low x otherwise the indefinite rise of F_2 would violate the unitarity bound. A study of the longitudinal structure function in the double scaling limit may be found in [12].

4. Large rapidity gap events

In approximately 10% of the events used to study F_2, a large rapidity gap in the hadronic final state was observed between the photon and the proton fragmentation regions. This is described in Figure 10. These events were fairly independent of W and Q^2. This implies that there is no energy or colour flow between the struck parton and the proton remnant direction. A generic explanation of these events is through the exchange of a colour

singlet parton which is typically a pomeron. Such events are typical of diffractive events through which one introduces the idea of the pomeron. For our purposes, the pomeron is the generic name for a particle the exchange of which is responsible for these large rapidity gap events.

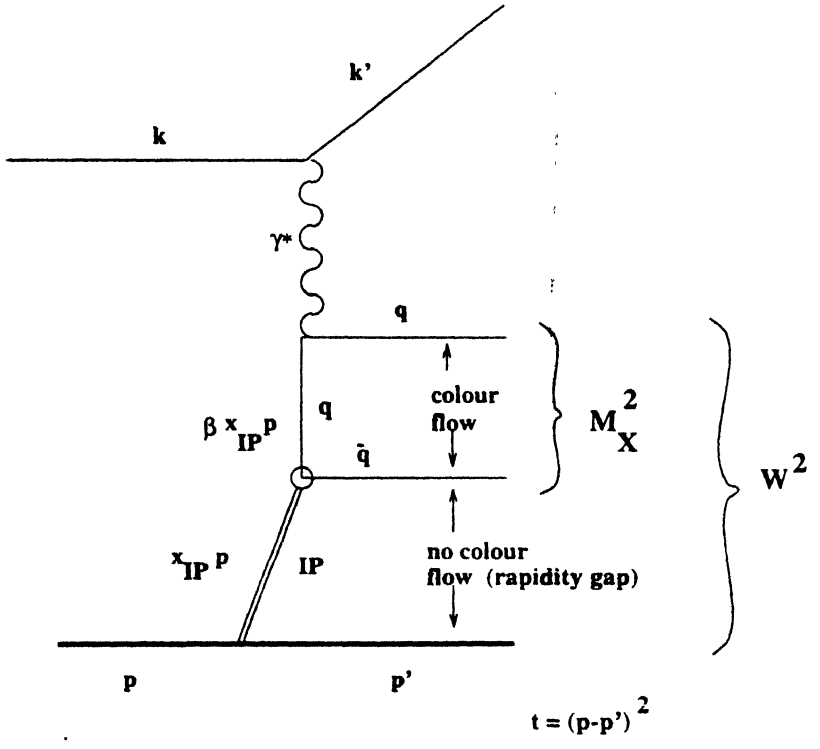

Figure 10. Schematic representation of a DIS event with a large rapidity gap as discussed in the text.

One of the simplest ways to understand these processes is to consider $\gamma^* p$ scattering in the rest frame of the proton. Here, the life time of a $\bar{q}q$ fluctuation of the virtual photon is given by $t \simeq 1/(2m_p x)$ where m_p is the mass of the proton. This time scale corresponds to a distance of $c\tau \simeq 10^3 fm$ for $x = 10^{-4}$ which is much larger that the typical size of a hadronic target. Thus the photon may fluctuate into a $q\bar{q}$ pair before arriving at the target, thereby making $\gamma^* p$ interaction similar to hadron hadron interaction. Diffractive scattering emerges as a consequence of the hadronic nature of the virtual photon.

It is important here to present the appropriate kinematic variables for the process. We use the variables x_{IP} for the fraction of the proton momentum carried by the generic pomeron IP, and β the fraction of the pomeron momentum carried by the struck quark with $\beta = x/x_{IP}$, x being the usual Bjorken variable. Neglecting the mass of the proton and taking $t \simeq 0$, see Figure 10)

$$x_{IP} = \frac{Q^2 + M_X^2}{W^2 + M_X^2}; \quad \beta = \frac{Q^2}{Q^2 + M_X^2}. \tag{20}$$

Assuming the validity of Regge factorization for $\gamma^* p$ diffractive interactions we have

$$\frac{d^2\sigma(\gamma^* p)}{dt\,dx_{IP}} = F_{IP/p}(t, x_{IP})\,\sigma(\gamma^* IP), \tag{21}$$

where $F_{IP/p}(t, x_{IP})$ is the flux of the pomeron in the proton. The DIS differential cross section for producing a diffractive hadronic state X of mass M_X is

$$\frac{d^3\sigma^D}{dx_{IP}\,d\beta dQ^2} = \frac{2\pi\alpha^2}{\beta Q^4}\left[1 + (1-y)^2\right] F_2^{D(3)}(\beta, Q^2, x_{IP}), \tag{22}$$

$F_2^{D(3)}$ denotes the contribution of diffractive events with a given x_{IP} integrated over t to the proton structure function F_2 for a given Q^2 and x. This part of the structure function is related to the pomeron structure function F_2^{IP} by

$$F_2^{D(3)}(\beta, Q^2, x_{IP}) = \frac{1}{x_{IP}^n} F_2^{IP}(\beta, Q^2), \tag{23}$$

where $n = 1 - 2a_{IP}(0) + d$, independent of b and Q^2.

H1 has carried out measurements of $x_{IP} F_2^{D(3)}$ in the range $2.5 < Q^2 < 65$ GeV^2, $0.01 < \beta < 0.9$ and $10^{-4} < x_{IP} < 5.10^{-2}$ and this is shown in Figure 11. The pomeron trajectory fit corresponds to an intercept

$$\alpha_{IP}(0) = 1.18 \pm 0.02 \pm 0.07, \tag{24}$$

which is somewhat higher than the intercept of a soft pomeron (~0.08). The result from ZEUS is similar

$$\alpha_{IP}(0) = 1.17 \pm 0.04 \pm 0.08. \tag{25}$$

The quantity $\tilde{F}_2^D = \int F_2^{D(3)} dx_{IP}$ is directly proportional to F_2^{IP} and is found to be almost independent of Q^2. This can be explained only by a large gluon contribution (see [13] for details). In fact more than 80% of the Pomeron momentum is carried away by hard gluons in the range of Q^2 being studied.

To summarise, the pomeron, which is a generic term to describe a colour singlet particle with vacuum quantum numbers, seems different in different processes. In particular, the pomeron in these diffractive events with large rapidity gaps seems to be harder than the usual soft pomeron of Donnachie and Landshoff [3]. Using DGLAP evolution it is found that the effective pomeron is made of mostly hard gluons. It is clear however, that the pomeron is not a universal object and has different intercepts in different processes.

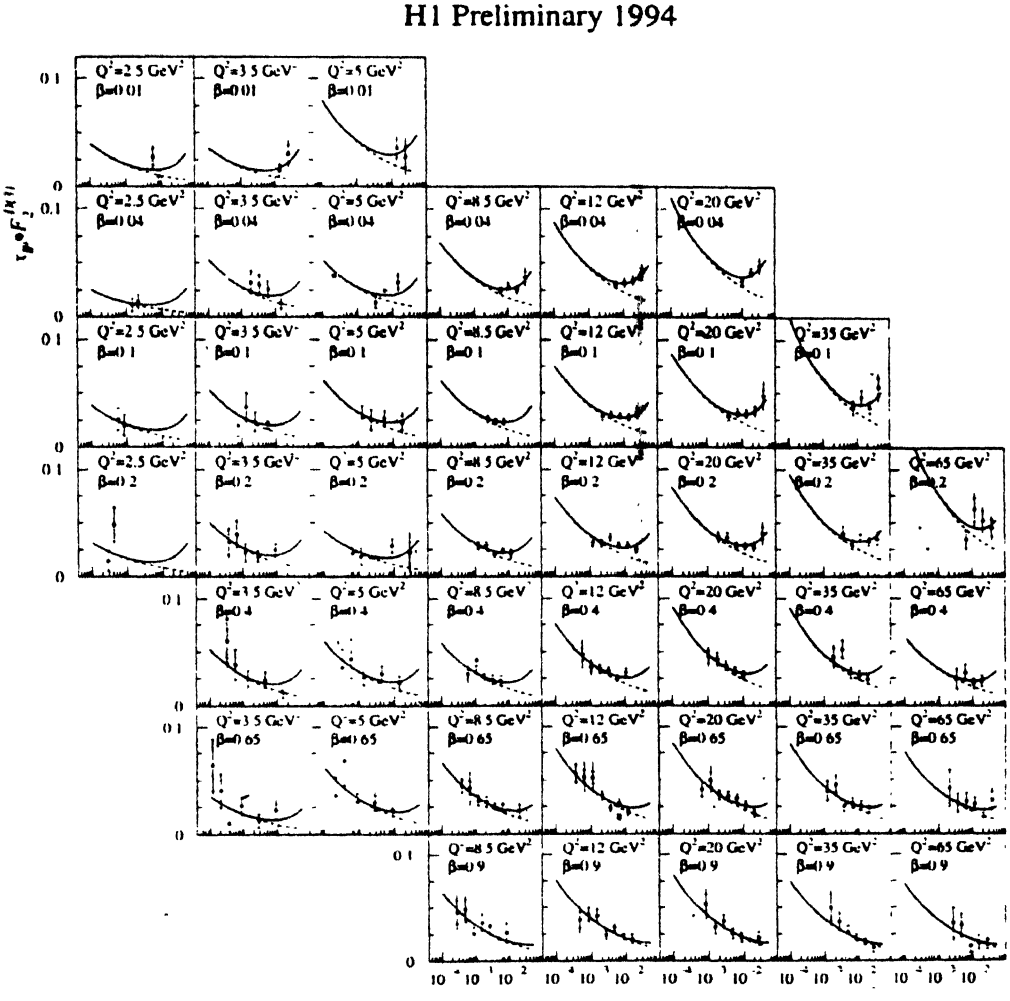

Figure 11. $x_{IP} F_2^{D(3)}$ as a function of x_{IP} in bins of β and Q^2 as denoted in the figure. The full line is the fit of an incoherent sum of the IP and f meson trajectories. The dashed line corresponds to the IP contribution. (from [13]).

5. Photon structure function

Even though a photon, being a gauge particle has no intrinsic structure, its hadronic fluctuations (through its interaction with matter) give it a partonic structure. Hard scattering processes (jets and charm production) yield tests of perturbative QCD at NLO and give information about the quark and gluon structure of the photon. We will very briefly touch upon some of these matters. 1 Large E_T dijet photoproduction takes places at leading order through the 'direct' scattering process $\hat{\sigma}(\gamma q \to qg) \otimes q^p$ and $\hat{\sigma}(\gamma q \to q\bar{q}) \otimes g^p$. There are also so-called resolved processes (at higher order) $\hat{\sigma}(gq \to gq) \otimes g^\gamma \otimes q^p$ and $\hat{\sigma}(qq \to qq) \otimes q^p \otimes q^\gamma$. The momentum fraction of the

photon constituent can be recontructed from the transverse energies and rapidities of the dijets,

$$x_\gamma = \frac{E_{T1} \exp(-\eta_1) + E_{T2} \exp(-\eta_2)}{2E_\gamma}. \tag{26}$$

Thus, 'direct' processes have $x_\gamma \approx 1$ and 'resolved' processes $x_g < 1$. The angular distribution of the dijets can also be measured to provide information on the nature of the hard scattering process. In fact, the expected difference in distribution between direct and resolved process can be clearly seen in the data and is again in good agreement with NLO QCD predictions. There are also a host of other results both from H1 and ZEUS. A good summary of the results and their theoretical implications can be found in the report of the photoproduction working group of the HERA workshop on proton, photon and pomeron structure function [14].

6. Exclusive vector meson production

The detectors at H1 and ZEUS have the ability to study the nature of the hadronic final state in detail. As a result there has been renewed interest in the study of J/ψ production at HERA. The production cross section for the process is dominated by photoproduction *i.e* by the interaction of almost real photons $Q^2 \approx 0$.

The process $\gamma p \rightarrow J/\psi X$ can take place through various mechanisms. The elastic process corresponds to $X = p$ for which there are various models proposed, in particular the soft pomeron picture of Donnachie and Landshoff [3] and the Ryskin model [15]. The Ryskin model is based on perturbative QCD and is an attempt to describe a hard pomeron through a gluon ladder of the BFKL kind. The elastic process can be with proton dissociation or without. In both cases, with small momentum transfer, the J/ψ particle retains the full photon energy ($z \approx 1$ with $z = E_\psi/E_\gamma$ in the proton rest frame). J/ψ production with proton dissociation also leads to z values close to one even though its strictly speaking, an inelastic process.

However, the principle inelastic process is that of photon-gluon fusion which has been modelled by Berger and Jones [17] who calculated this in perturbative QCD due to the hard scale given by the mass of the charm quark. In the colour singlet model for photoproduction of J/ψ which is based on the Berger-Jones picture, the formation of the J/ψ state is accompanied by the emission of a hard gluon. A comparison of the colour singlet model to data gave a discrepancy in absolute magnitude which was attributed to missing higher order calculations (also called the "K-factor"). Subsequently, several improvements including a complete NLO calculation [18] have been performed and compared successfully with the data. The possibility of colour octet contributions have also been studied for an overview, see, for example, [19]. All these various processes are shown diagramatically in Figure 12. There is not enough space to show the data for J/ψ production. The interested reader is referred to [20] for data and experimental details. We will only briefly describe the data. The data show a rise with $W_{\gamma p}$ which in the HERA

regime can be modelled by $\delta_{\gamma p} \propto W_{\gamma p}^{\delta}$. A fit to the HERA data gives $\delta = 0.64 \pm 0.13$ (including systematic and statistical errors). Using also the ZEUS data and lower energies, gives $\delta = 0.90 \pm 0.06$.

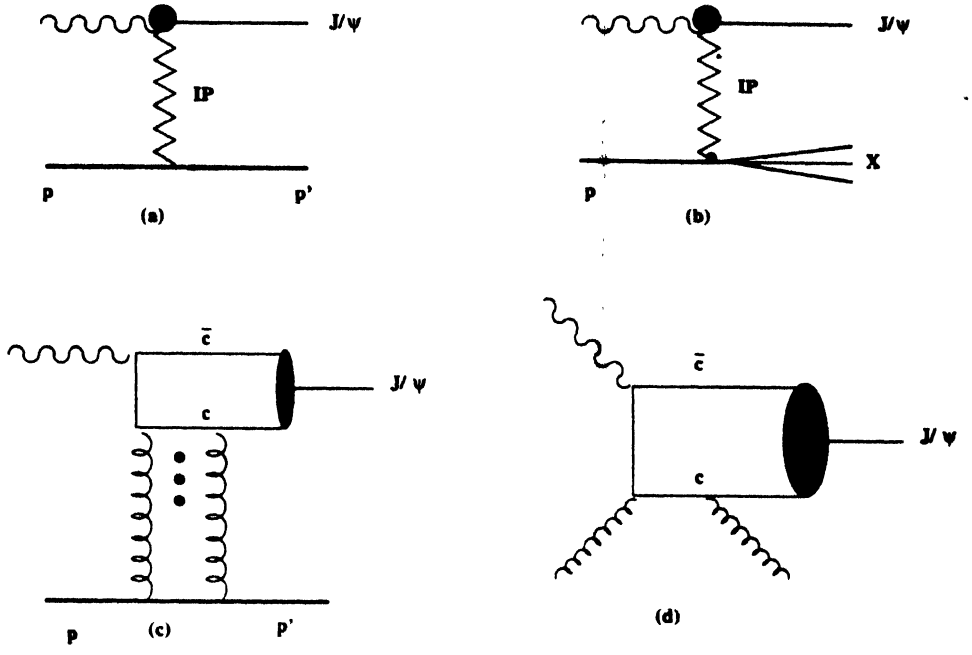

Figure 12. J/ψ production mechanisms : (a) elastic J/ψ production *via* pomeron exchange, (b) diffractive proton dissociation, (c) elastic J/ψ production in perturbative QCD (Ryskin model, see text), (d)photon gluon fusion model for inelastic J/ψ production in colour singlet model.

The energy dependence from the Donnachie-Landshoff [3] soft pomeron model corresponds to $\delta = 0.32$. The Donnachie-Landshoff prediction falls well below the data by a factor of 3 or so. The prediction of the QCD-based model of Ryskin and including higher order corrections [16] gives much better agreement in general. The Ryskin model, based as it is on a 2 gluon ladder, depends quadratically on the gluon distribution taken at the scale $(Q^2 + m_\psi^2)/4 \approx 2.4\ \text{GeV}^2$. The distribution at this scale can be parametrised by $xg(x) \propto x^{-\lambda}$. For values of $x \approx m_\psi^2 / W_{\gamma p}^2 \approx 10^{-3}$ the gluon distribution from MRSA' [21] corresponds to $\lambda \approx 0.2$ which gives good agreement with data between 10 and 150 GeV. The GkV parametrisation [4] corresponds to $\lambda \approx 0.3$–0.4 giving a curve with a somewhat steeper energy dependence than the data.

The inelastic data sample is selected by requiring $0.45 \leq z \leq 0.90$ to reject elastic (diffractive) and resolved photon events. The inputs are the charm mass $m_c = 1.4$ GeV, $\Lambda_{\overline{\text{MS}}} = 300$ MeV and the renormalisation scale is chosen to be the factorisation scale $\sqrt{2}m_c$. Once again the gluon distributions at low x can be parametrised by $xg(x) \propto x^{-\lambda}$ with λ ranging from 0 (MRSD0') [22] to 0.4 (MRSG) [21]. Approximate agreement is seen, however the data cover a wide range in absolute normalisation. Since the NLO

corrections are not fully under control for $p_t^2 \to 0$ and $z \to 1$, a restricted kinematic sample with $z < 0.8$ and $p_t^2 > 1$ GeV^2 has been studied by experimentalists. There is improved agreement for all the gluon distributions but the sensitivity is reduced. Again, details may be found in [20] An application of the asymptotic form of the gluon distribution as obtained from the double scaling limit to both the inelastic and elastic regions may be found in [23].

To summarise, once again, the agreement with data is very good with standard gluon parametrisations, provided a hard pomeron (as that built up of gluon ladders as in the Ryskin model) is used. This picture explains the diffractive/elastic events far better than the soft pomeron version of Donnachie and Landshoff [3] In the elastic case the Berger and Jones picture using the colour singlet model of J/ψ production seems to give a satisfactory description of the data once NLO corrections are included and suitable cuts on z and p_t^2 and incorporated.

7. Conclusion

The structure function F_2 has now been measured in the kinematic range $10^{-6} < x < 0.85$ and $0.1 < Q^2 < 30{,}000$ GeV^2. The rise of F_2 with decreasing x is well explained by conventional DGLAP evolution but also by non-conventional dynamics like BFKL. A less inclusive measurement is required to distinguish these different evolution equations. The large rapidity gap events and diffractive scattering show that the (generic) pomeron is different in different processes but is harder than the Donnachie-Landshoff soft pomeron. Exclusive vector meson production also indicates that both for inelastic and elastic/diffractive events, perturbative QCD based descriptions explain the data fairly well. LEP and HERA have also given us the low x regime of the partonic structure of the photon, even though lack of space has not allowed me to discuss these aspects. The next frontier is that of polarised DIS at low x. The HERMES experiment is a step in that direction.

The large body of theoretical work on low x has given us a good understanding of QCD dynamics at large parton densities. As a result, parton densities are now available over a large range in Q^2 and x. The results from HERA have given us new ways to connect partonic and hadronic degrees of freedom and contributed to a major improvement in our understanding of the short distance structure of hadrons. Low x QCD is one of the few areas of particle physics where theorists have had to work hard to keep up with experimentalists.

Due to constraints of space, I have left out many other aspects of HERA Physics, like photon structure functions, charged current interactions, some aspects of jets in photoproduction *etc*. The HERA Workshop on proton, photon and pomeron structure [24] discusses in detail many of the issues touched upon here as well as some of the other experimental results that have not been discussed here.

Acknowledgments

I would like to thank the organisers of the XII DAE symposium on High Energy Physics for inviting me to give this talk and for hospitality during the symposium.

References

[1] H1 Collaboration; T Ahmed *et al Nucl. Phys.* **B429** 477 (1994); S Aid *et al Nucl. Phys.* **B470** 3 (1996)

[2] ZEUS Collaboration; M Derrick *et al Phys. Lett.* **B315** 481 (1993); Z. *Phys.* **C69** 607 (1996)

[3] A Donnachie and P V Landshoff *Nucl. Phys.* **B231** 189 (1983); *ibid.* **B244** 322 (1984); *ibid.* **B267** 690 (1986); *Phys. Lett.* **B296** 227 (1992); *ibid* **B202** 131 (1988)

[4] M Gluck, E Reya and A Vogt Z. *Phys.* **C67** 433 (1995)

[5] A D Martin, W J Stirling and R G Roberts *Phys. Rev.* **D50** 6734 (1994)

[6] Y L Dokshitzer *Sov. Phys. JETP* **46** 641 (1977)

[7] V N Gribov and L N Lipatov *Sov. J. Nucl. Phys.* **15** 438 675 (1972); G Altarelli and G Parisi *Nucl. Phys.* **B126** 298 (1977)

[8] V Fadin, E Kuraev and L Lipatov *Sov. Phys. JETP* **44** 443 (1976); *ibid.* **45** 199 (1977); Y Balitski and L Lipatov *Sov. J. Nucl. Phys.* **28** 822 (1978)

[9] A H Mueller *Nucl. Phys.* B (*Proc. Suppl.*), **18C** 125 (1990); *J. Phys.* **G17** 1443 (1991)

[10] *Working Group Report on the Structure of the Proton* B Badelek *et al J. Phys.* **G22** 815 (in particular, see section 5.5) (1996)

[11] R D Ball and S Forte *Phys. Lett.* **B335** 77 (1994); *Phys. Lett.* **B336** 77 (1994)

[12] T Sarkar and Rahul Basu *hep-ph/9607232 Phys. Lett. B* (submitted) (1999)

[13] H Abramowicz *Tests of QCD at Low x-hep-ex/9612001 Proceedings of the 28th International Conference on High Energy Physics*, 1996 (Warsaw) (to be published) (1999)

[14] *Photoproduction Working Group Report, HERA Workshop on Proton, Photon and Pomeron Structure Function J. Phys.* **G22** 871 (1996)

[15] M G Ryskin Z. *Phys.* **C57** 89 (1993)

[16] M G Ryskin *et al preprint DTP/95/96, CBPF-NF-079/95, RAL-TR-95-065, hep-ph/9511228* (1995), revised February (1996)

[17] E I Berger and D Jones *Phys. Rev.* **D23** 1521 (1981)

[18] M Kramer *hep-ph/9508409, Nucl. Phys.* **B459** 3 (1996)

[19] M Cacciari and M Kramer *hep-ph/9601276, DESY preprint DESY 96-005*

[20] H1 Collaboration; S Aid *et al Nucl. Phys.* **B472** 3 (hep-ex/9603005) (1996)

[21] A D Martin, R G Roberts and W J Stirling *Phys. Lett.* **B354** 155 (1995)

[22] A D Martin, W J Stirling and R G Roberts *Phys. Lett.* **B306** 145 (1993); *ibid.* **B309** 492 (1993)

[23] T Sarkar and Rahul Basu *hep-ph/9701337 Phys. Lett. B* (submitted)

[24] *HERA Workshop on Proton, Photon and Pomeron Structure, J. Phys.* **G22** 669 (1996)